DESY 96-067
April 1996

Measurement of the Reaction $\gamma^* p \to \phi p$ in Deep Inelastic $e^+ p$ Scattering at HERA

ZEUS Collaboration

Abstract

The production of ϕ mesons in the reaction $e^+ p \to e^+ \phi p$ ($\phi \to K^+ K^-$), for $7 < Q^2 < 25$ GeV^2 and for virtual photon-proton centre of mass energies (W) in the range 42-134 GeV, has been studied with the ZEUS detector at HERA. When compared to lower energy data at similar Q^2, the results show that the $\gamma^* p \to \phi p$ cross section rises strongly with W. This behaviour is similar to that previously found for the $\gamma^* p \to \rho^0 p$ cross section. This strong dependence cannot be explained by production through soft pomeron exchange. It is, however, consistent with perturbative QCD expectations, where it reflects the rise of the gluon momentum density in the proton at small x. The ratio of $\sigma(\phi)/\sigma(\rho^0)$, which has previously been determined by ZEUS to be 0.065 ± 0.013 (stat.) in photoproduction at a mean W of 70 GeV, is measured to be 0.18 ± 0.05 (stat.) ± 0.03 (syst.) at a mean Q^2 of 12.3 GeV^2 and mean W of ≈ 100 GeV and is thus approaching at large Q^2 the value of 2/9 predicted from the quark charges of the vector mesons and a flavour independent production mechanism.

The ZEUS Collaboration

M. Derrick, D. Krakauer, S. Magill, D. Mikunas, B. Musgrave, J.R. Okrasinski, J. Repond, R. Stanek, R.L. Talaga, H. Zhang
Argonne National Laboratory, Argonne, IL, USA [p]

M.C.K. Mattingly
Andrews University, Berrien Springs, MI, USA

G. Bari, M. Basile, L. Bellagamba, D. Boscherini, A. Bruni, G. Bruni, P. Bruni, G. Cara Romeo, G. Castellini[1], L. Cifarelli[2], F. Cindolo, A. Contin, M. Corradi, I. Gialas, P. Giusti, G. Iacobucci,
G. Laurenti, G. Levi, A. Margotti, T. Massam, R. Nania, F. Palmonari, A. Polini, G. Sartorelli, Y. Zamora Garcia[3], A. Zichichi
University and INFN Bologna, Bologna, Italy [f]

C. Amelung, A. Bornheim, J. Crittenden, R. Deffner, T. Doeker[4], M. Eckert, L. Feld, A. Frey[5], M. Geerts, M. Grothe, H. Hartmann, K. Heinloth, L. Heinz, E. Hilger, H.-P. Jakob, U.F. Katz, S. Mengel[6], E. Paul, M. Pfeiffer, Ch. Rembser, D. Schramm[7], J. Stamm, R. Wedemeyer
Physikalisches Institut der Universität Bonn, Bonn, Germany [c]

S. Campbell-Robson, A. Cassidy, W.N. Cottingham, N. Dyce, B. Foster, S. George, M.E. Hayes,
G.P. Heath, H.F. Heath, D. Piccioni, D.G. Roff, R.J. Tapper, R. Yoshida
H.H. Wills Physics Laboratory, University of Bristol, Bristol, U.K. [o]

M. Arneodo[8], R. Ayad, M. Capua, A. Garfagnini, L. Iannotti, M. Schioppa, G. Susinno
Calabria University, Physics Dept.and INFN, Cosenza, Italy [f]

A. Caldwell[9], N. Cartiglia, Z. Jing, W. Liu, J.A. Parsons, S. Ritz[10], F. Sciulli, P.B. Straub, L. Wai[11], S. Yang[12], Q. Zhu
Columbia University, Nevis Labs., Irvington on Hudson, N.Y., USA [q]

P. Borzemski, J. Chwastowski, A. Eskreys, Z. Jakubowski, M.B. Przybycień, M. Zachara, L. Zawiejski
Inst. of Nuclear Physics, Cracow, Poland [j]

L. Adamczyk, B. Bednarek, K. Jeleń, D. Kisielewska, T. Kowalski, M. Przybycień, E. Rulikowska-Zarębska, L. Suszycki, J. Zając
Faculty of Physics and Nuclear Techniques, Academy of Mining and Metallurgy, Cracow, Poland [j]

Z. Duliński, A. Kotański
Jagellonian Univ., Dept. of Physics, Cracow, Poland [k]

G. Abbiendi[13], L.A.T. Bauerdick, U. Behrens, H. Beier, J.K. Bienlein, G. Cases, O. Deppe, K. Desler, G. Drews, M. Flasiński[14], D.J. Gilkinson, C. Glasman, P. Göttlicher, J. Große-Knetter, T. Haas, W. Hain, D. Hasell, H. Heßling, Y. Iga, K.F. Johnson[15], P. Joos, M. Kasemann, R. Klanner, W. Koch, U. Kötz, H. Kowalski, J. Labs, A. Ladage, B. Löhr, M. Löwe, D. Lüke, J. Mainusch[16], O. Mańczak, J. Milewski, T. Monteiro[17], J.S.T. Ng, D. Notz, K. Ohrenberg, K. Piotrzkowski, M. Roco, M. Rohde, J. Roldán, U. Schneekloth, W. Schulz, F. Selonke, B. Surrow, T. Voß, D. Westphal, G. Wolf, U. Wollmer,
C. Youngman, W. Zeuner
Deutsches Elektronen-Synchrotron DESY, Hamburg, Germany

H.J. Grabosch, A. Kharchilava[18], S.M. Mari[19], A. Meyer, S. Schlenstedt, N. Wulff
DESY-IfH Zeuthen, Zeuthen, Germany

G. Barbagli, E. Gallo, P. Pelfer
University and INFN, Florence, Italy [f]

G. Maccarrone, S. De Pasquale, L. Votano
INFN, Laboratori Nazionali di Frascati, Frascati, Italy [f]

A. Bamberger, S. Eisenhardt, T. Trefzger, S. Wölfle
Fakultät für Physik der Universität Freiburg i.Br., Freiburg i.Br., Germany [c]

J.T. Bromley, N.H. Brook, P.J. Bussey, A.T. Doyle, D.H. Saxon, L.E. Sinclair, M.L. Utley, A.S. Wilson
Dept. of Physics and Astronomy, University of Glasgow, Glasgow, U.K. [o]

A. Dannemann, U. Holm, D. Horstmann, R. Sinkus, K. Wick
Hamburg University, I. Institute of Exp. Physics, Hamburg, Germany [c]

B.D. Burow[20], L. Hagge[16], E. Lohrmann, N. Pavel, G. Poelz, W. Schott, F. Zetsche
Hamburg University, II. Institute of Exp. Physics, Hamburg, Germany [c]

T.C. Bacon, N. Brümmer, I. Butterworth, V.L. Harris, G. Howell, B.H.Y. Hung, L. Lamberti[21], K.R. Long, D.B. Miller, A. Prinias[22], J.K. Sedgbeer, D. Sideris, A.F. Whitfield
Imperial College London, High Energy Nuclear Physics Group, London, U.K. [o]

U. Mallik, M.Z. Wang, S.M. Wang, J.T. Wu
University of Iowa, Physics and Astronomy Dept., Iowa City, USA [p]

P. Cloth, D. Filges
Forschungszentrum Jülich, Institut für Kernphysik, Jülich, Germany

S.H. An, G.H. Cho, B.J. Ko, S.B. Lee, S.W. Nam, H.S. Park, S.K. Park
Korea University, Seoul, Korea [h]

S. Kartik, H.-J. Kim, R.R. McNeil, W. Metcalf, V.K. Nadendla
Louisiana State University, Dept. of Physics and Astronomy, Baton Rouge, LA, USA [p]

F. Barreiro, J.P. Fernandez, R. Graciani, J.M. Hernández, L. Hervás, L. Labarga, M. Martinez, J. del Peso, J. Puga, J. Terron, J.F. de Trocóniz
Univer. Autónoma Madrid, Depto de Física Teóríca, Madrid, Spain [n]

F. Corriveau, D.S. Hanna, J. Hartmann, L.W. Hung, J.N. Lim, C.G. Matthews[23], P.M. Patel, M. Riveline, D.G. Stairs, M. St-Laurent, R. Ullmann, G. Zacek
McGill University, Dept. of Physics, Montréal, Québec, Canada [a], [b]

T. Tsurugai
Meiji Gakuin University, Faculty of General Education, Yokohama, Japan

V. Bashkirov, B.A. Dolgoshein, A. Stifutkin
Moscow Engineering Physics Institute, Mosocw, Russia [l]

G.L. Bashindzhagyan[24], P.F. Ermolov, L.K. Gladilin, Yu.A. Golubkov, V.D. Kobrin, I.A. Korzhavina, V.A. Kuzmin, O.Yu. Lukina, A.S. Proskuryakov, A.A. Savin, L.M. Shcheglova, A.N. Solomin, N.P. Zotov
Moscow State University, Institute of Nuclear Physics, Moscow, Russia [m]

M. Botje, F. Chlebana, J. Engelen, M. de Kamps, P. Kooijman, A. Kruse, A. van Sighem, H. Tiecke, W. Verkerke, J. Vossebeld, M. Vreeswijk, L. Wiggers, E. de Wolf, R. van Woudenberg[25]
NIKHEF and University of Amsterdam, Netherlands [i]

D. Acosta, B. Bylsma, L.S. Durkin, J. Gilmore, C. Li, T.Y. Ling, P. Nylander, I.H. Park, T.A. Romanowski[26]
Ohio State University, Physics Department, Columbus, Ohio, USA [p]

D.S. Bailey, R.J. Cashmore[27], A.M. Cooper-Sarkar, R.C.E. Devenish, N. Harnew, M. Lancaster[28], L. Lindemann, J.D. McFall, C. Nath, V.A. Noyes[22], A. Quadt, J.R. Tickner, H. Uijterwaal, R. Walczak, D.S. Waters, F.F. Wilson, T. Yip
Department of Physics, University of Oxford, Oxford, U.K. [o]

A. Bertolin, R. Brugnera, R. Carlin, F. Dal Corso, M. De Giorgi, U. Dosselli, S. Limentani, M. Morandin, M. Posocco, L. Stanco, R. Stroili, C. Voci, F. Zuin
Dipartimento di Fisica dell' Universita and INFN, Padova, Italy [f]

J. Bulmahn, R.G. Feild[29], B.Y. Oh, J.J. Whitmore
Pennsylvania State University, Dept. of Physics, University Park, PA, USA [q]

G. D'Agostini, G. Marini, A. Nigro, E. Tassi
Dipartimento di Fisica, Univ. 'La Sapienza' and INFN, Rome, Italy [f]

J.C. Hart, N.A. McCubbin, T.P. Shah
Rutherford Appleton Laboratory, Chilton, Didcot, Oxon, U.K. [o]

E. Barberis, T. Dubbs, C. Heusch, M. Van Hook, W. Lockman, J.T. Rahn, H.F.-W. Sadrozinski, A. Seiden, D.C. Williams
University of California, Santa Cruz, CA, USA [p]

J. Biltzinger, R.J. Seifert, O. Schwarzer, A.H. Walenta, G. Zech
Fachbereich Physik der Universität-Gesamthochschule Siegen, Germany [c]

H. Abramowicz, G. Briskin, S. Dagan[30], A. Levy[24]
School of Physics, Tel-Aviv University, Tel Aviv, Israel [e]

J.I. Fleck[31], M. Inuzuka, T. Ishii, M. Kuze, S. Mine, M. Nakao, I. Suzuki, K. Tokushuku, K. Umemori, S. Yamada, Y. Yamazaki
Institute for Nuclear Study, University of Tokyo, Tokyo, Japan [g]

M. Chiba, R. Hamatsu, T. Hirose, K. Homma, S. Kitamura[32], T. Matsushita, K. Yamauchi
Tokyo Metropolitan University, Dept. of Physics, Tokyo, Japan [g]

R. Cirio, M. Costa, M.I. Ferrero, S. Maselli, C. Peroni, R. Sacchi, A. Solano, A. Staiano
Universita di Torino, Dipartimento di Fisica Sperimentale and INFN, Torino, Italy [f]

M. Dardo
II Faculty of Sciences, Torino University and INFN - Alessandria, Italy [f]

D.C. Bailey, F. Benard, M. Brkic, C.-P. Fagerstroem, G.F. Hartner, K.K. Joo, G.M. Levman, J.F. Martin, R.S. Orr, S. Polenz, C.R. Sampson, D. Simmons, R.J. Teuscher
University of Toronto, Dept. of Physics, Toronto, Ont., Canada [a]

J.M. Butterworth, C.D. Catterall, T.W. Jones, P.B. Kaziewicz, J.B. Lane, R.L. Saunders, J. Shulman, M.R. Sutton
University College London, Physics and Astronomy Dept., London, U.K. [o]

B. Lu, L.W. Mo
Virginia Polytechnic Inst. and State University, Physics Dept., Blacksburg, VA, USA [q]

W. Bogusz, J. Ciborowski, J. Gajewski, G. Grzelak[33], M. Kasprzak, M. Krzyżanowski, K. Muchorowski[34], R.J. Nowak, J.M. Pawlak, T. Tymieniecka, A.K. Wróblewski, J.A. Zakrzewski, A.F. Żarnecki
Warsaw University, Institute of Experimental Physics, Warsaw, Poland [j]

M. Adamus
Institute for Nuclear Studies, Warsaw, Poland [j]

C. Coldewey, Y. Eisenberg[30], D. Hochman, U. Karshon[30], D. Revel[30], D. Zer-Zion
Weizmann Institute, Nuclear Physics Dept., Rehovot, Israel [d]

W.F. Badgett, J. Breitweg, D. Chapin, R. Cross, S. Dasu, C. Foudas, R.J. Loveless, S. Mattingly, D.D. Reeder, S. Silverstein, W.H. Smith, A. Vaiciulis, M. Wodarczyk
University of Wisconsin, Dept. of Physics, Madison, WI, USA [p]

S. Bhadra, M.L. Cardy, W.R. Frisken, M. Khakzad, W.N. Murray, W.B. Schmidke
York University, Dept. of Physics, North York, Ont., Canada [a]

[1] also at IROE Florence, Italy
[2] now at Univ. of Salerno and INFN Napoli, Italy
[3] supported by Worldlab, Lausanne, Switzerland
[4] now as MINERVA-Fellow at Tel-Aviv University
[5] now at Univ. of California, Santa Cruz
[6] now at VDI-Technologiezentrum Düsseldorf
[7] now at ESG, München
[8] also at University of Torino and Alexander von Humboldt Fellow
[9] Alexander von Humboldt Fellow
[10] Alfred P. Sloan Foundation Fellow
[11] now at University of Washington, Seattle
[12] now at California Institute of Technology, Los Angeles
[13] supported by an EC fellowship number ERBFMBICT 950172
[14] now at Inst. of Computer Science, Jagellonian Univ., Cracow
[15] visitor from Florida State University
[16] now at DESY Computer Center
[17] supported by European Community Program PRAXIS XXI
[18] now at Univ. de Strasbourg
[19] present address: Dipartimento di Fisica, Univ. "La Sapienza", Rome
[20] also supported by NSERC, Canada
[21] supported by an EC fellowship
[22] PPARC Post-doctoral Fellow
[23] now at Park Medical Systems Inc., Lachine, Canada
[24] partially supported by DESY
[25] now at Philips Natlab, Eindhoven, NL
[26] now at Department of Energy, Washington
[27] also at University of Hamburg, Alexander von Humboldt Research Award
[28] now at Lawrence Berkeley Laboratory, Berkeley
[29] now at Yale University, New Haven, CT
[30] supported by a MINERVA Fellowship
[31] supported by the Japan Society for the Promotion of Science (JSPS)
[32] present address: Tokyo Metropolitan College of Allied Medical Sciences, Tokyo 116, Japan
[33] supported by the Polish State Committee for Scientific Research, grant No. 2P03B09308
[34] supported by the Polish State Committee for Scientific Research, grant No. 2P03B09208

[a] supported by the Natural Sciences and Engineering Research Council of Canada (NSERC)
[b] supported by the FCAR of Québec, Canada
[c] supported by the German Federal Ministry for Education and Science, Research and Technology (BMBF), under contract numbers 056BN19I, 056FR19P, 056HH19I, 056HH29I, 056SI79I
[d] supported by the MINERVA Gesellschaft für Forschung GmbH, the Israel Academy of Science and the U.S.-Israel Binational Science Foundation
[e] supported by the German Israeli Foundation, and by the Israel Academy of Science
[f] supported by the Italian National Institute for Nuclear Physics (INFN)
[g] supported by the Japanese Ministry of Education, Science and Culture (the Monbusho) and its grants for Scientific Research
[h] supported by the Korean Ministry of Education and Korea Science and Engineering Foundation
[i] supported by the Netherlands Foundation for Research on Matter (FOM)
[j] supported by the Polish State Committee for Scientific Research, grants No. 115/E-343/SPUB/P03/109/95, 2P03B 244 08p02, p03, p04 and p05, and the Foundation for Polish-German Collaboration (proj. No. 506/92)
[k] supported by the Polish State Committee for Scientific Research (grant No. 2 P03B 083 08) and Foundation for Polish-German Collaboration
[l] partially supported by the German Federal Ministry for Education and Science, Research and Technology (BMBF)
[m] supported by the German Federal Ministry for Education and Science, Research and Technology (BMBF), and the Fund of Fundamental Research of Russian Ministry of Science and Education and by INTAS-Grant No. 93-63
[n] supported by the Spanish Ministry of Education and Science through funds provided by CICYT
[o] supported by the Particle Physics and Astronomy Research Council
[p] supported by the US Department of Energy
[q] supported by the US National Science Foundation

1 Introduction

The elastic photoproduction of ϕ mesons, $\gamma p \to \phi p$, has been studied in fixed target experiments [1, 2, 3] and at HERA [4] for photon-proton centre of mass (c.m.) energies (W) up to 70 GeV. For $W > 10$ GeV, the reaction $\gamma p \to \phi p$ displays the characteristics of a soft diffractive process: s-channel helicity conservation, a cross section rising weakly with W and an exponential t dependence (where t is the four-momentum transfer squared at the proton vertex) with a slope $b(W)$ which is also increasing slowly with W. Soft diffraction can be described by the exchange of a 'soft' pomeron Regge trajectory $\alpha(t) = \alpha(0) + \alpha' t$ with an intercept $\alpha(0) = 1.08$ and slope $\alpha' = 0.25$ GeV^{-2}. The intercept is determined from fits [5] to hadron-hadron total cross sections. The same intercept also describes the energy dependence of the photon-proton total cross section [6]. In addition, soft diffraction and the Vector Dominance Model can describe the energy dependence of both ϕ [4] and ρ^0 [7] elastic photoproduction at HERA energies.

In contrast, the same soft pomeron fails to describe the recently measured energy dependences of the cross sections at HERA for elastic J/ψ photoproduction [8] and the exclusive production of ρ^0 mesons [9, 10] in deep inelastic scattering (DIS) at large values of Q^2, the negative of the four-momentum transfer squared of the exchanged virtual photon. It also fails to describe the inclusive DIS diffractive cross section [11]. The rapid rise with energy of the cross sections for exclusive vector meson production is consistent with recent perturbative QCD (pQCD) calculations [12, 13, 14] in which the pomeron is treated as a perturbative two-gluon exchange. In such calculations the large scale may be the mass of the vector meson for J/ψ photoproduction [12], the Q^2 for exclusive DIS vector meson production [13] or a large value of t [14].

Brodsky et al. [13] have studied the forward scattering cross section for DIS exclusive vector meson production by applying pQCD in the double leading logarithm approximation (DLLA). At high Q^2 and small Bjorken x the vector mesons are expected to be produced dominantly by longitudinally polarised virtual photons with a dependence for the longitudinal part of the differential cross section:

$$\left.\frac{d\sigma_L}{dt}\right|_{t=0} (\gamma^* N \to V^0 N) = \frac{A}{Q^6}\alpha_s^2(Q^2) \cdot \left| \left[1 + i\frac{\pi}{2}\left(\frac{d}{d\ ln\ x}\right)\right] xg(x,Q^2)\right|^2, \qquad (1)$$

where A is a calculable constant and $xg(x,Q^2)$ is the momentum density of the gluon in the proton. In view of the rapid rise of $xg(x)$ at small x, as derived from HERA data [15], Eq. (1) predicts a rapid rise of the cross section versus W at fixed Q^2, substantially faster than the $W^{0.22}$ dependence expected for soft pomeron exchange. The predicted Q^2 behaviour resulting from Eq. (1) is, however, weaker than Q^{-6} as the combined Q^2 dependences of the strong coupling constant and the gluon momentum density provide an additional factor of $\sim Q^{1-2}$ to the Q^2 dependence.

From the quark charges of the vector mesons and a flavour independent production mechanism, the ratio $\sigma(\phi)/\sigma(\rho^0)$ of exclusive production cross sections is expected to be 2/9 [16]. The pQCD prediction increases from 2/9 to 2.4/9.0 at asymptotically large Q^2 [13, 17, 18]. Experimentally, for photoproduction the ratio is found to be 0.076 ± 0.010 at $W = 17$ GeV [3] and 0.065 ± 0.013 at 70 GeV [4]. At larger Q^2, NMC has determined that $\sigma(\phi)/\sigma(\rho^0)$ is ≈ 0.1 for $2 < Q^2 < 10$ GeV^2 [19]. The NMC measurements are for $W \approx 15$ GeV. It is of interest to determine this ratio at both large Q^2 and large W.

This letter reports a measurement of the exclusive cross section for ϕ mesons produced at large Q^2 by the process $\gamma^* p \to \phi p$ at HERA. The data come from neutral current, deep inelastic positron-proton scattering:

$$e^+ p \to e^+ \phi p \tag{2}$$

in the Q^2 range 7 - 25 GeV^2, similar to that of the earlier fixed target experiments [19, 20]. However, they cover a lower Bjorken x region ($4 \cdot 10^{-4} < x < 1 \cdot 10^{-2}$) or, equivalently, a higher W region (42-134 GeV). The ratio of $\sigma(\phi)/\sigma(\rho^0)$ is obtained by comparison to the ZEUS ρ^0 measurement [9] at similar Q^2 values and the helicity decay distribution is studied.

2 Experimental setup

2.1 HERA

During 1994 HERA operated with a proton beam energy (E_p) of 820 GeV and a positron beam energy (E_e) of 27.52 GeV. The positron and proton beams contained 153 colliding bunches together with additional 17 proton and 15 positron unpaired bunches. These additional bunches were used for background studies. The time between bunch crossings was 96 ns. The typical instantaneous luminosity was $1.5 \cdot 10^{30}$ cm^{-2}s^{-1}. The integrated luminosity for this study was 2.62 pb^{-1}, known to an accuracy of 0.08 pb^{-1}.

2.2 The ZEUS detector

A detailed description of the ZEUS detector can be found elsewhere [21]. The main components used in this analysis are outlined below.

Charged particle momenta are reconstructed by the vertex detector (VXD) [22] and the central tracking detector (CTD) [23]. These are cylindrical drift chambers placed in a magnetic field of 1.43 T produced by a thin superconducting coil. The vertex detector surrounds the beam pipe and consists of 120 radial cells, each with 12 sense wires. The CTD surrounds the vertex detector and consists of 72 cylindrical layers, organized in 9 superlayers covering the polar angle[1] region $15^o < \theta < 164^o$. Using the information from the CTD and the VXD for the two-track events of this analysis, the event vertex can be reconstructed with a resolution of 0.4 cm in Z. The transverse momentum resolution for tracks traversing all superlayers is $\sigma(p_T)/p_T \simeq \sqrt{(0.005 p_T)^2 + (0.016)^2}$, with p_T in GeV.

The high resolution uranium-scintillator calorimeter CAL [24] is divided into three parts, the forward (proton direction) calorimeter (FCAL), the barrel calorimeter (BCAL) and the rear (positron direction) calorimeter (RCAL), which cover polar angles from 2.6^o to 36.7^o, 36.7^o to 129.1^o, and 129.1^o to 176.2^o, respectively. Each part consists of towers which are longitudinally subdivided into electromagnetic (EMC) and hadronic (HAC) readout cells. The transverse sizes are approximately 5×20 cm^2 for the EMC cells (10×20 cm^2 in RCAL) and 20×20 cm^2 for the HAC cells. From test beam data, energy resolutions of $\sigma_E/E = 0.18/\sqrt{E}$ for electrons and

[1]The ZEUS coordinate system has positive-Z in the direction of flight of the protons and the X-axis is horizontal, pointing towards the center of HERA. The nominal interaction point is at X = Y = Z = 0.

$\sigma_E/E = 0.35/\sqrt{E}$ for hadrons have been obtained (with E in GeV). In addition, the calorimeter cells provide time measurements with a time resolution below 1 ns for energy deposits greater than 4.5 GeV, a property used in background rejection.

The position of positrons scattered at small angles with respect to the positron beam direction is determined by the Small-angle Rear Tracking Detector (SRTD) which is attached to the front face of the RCAL. The SRTD consists of two planes of scintillator strips, 1 cm wide and 0.5 cm thick, arranged in orthogonal directions and read out via optical fibres and photomultiplier tubes. It covers the region of 68×68 cm^2 in X and Y. A hole of 20×20 cm^2 at the centre accommodates the beampipe. The SRTD is able to resolve clearly single minimum ionising particles and has a position resolution of 0.3 cm and a timing resolution of better than 2 ns.

The luminosity was determined from the rate of the Bethe-Heitler process $e^+p \to e^+\gamma p$, where the photon is measured by a calorimeter [25] located at Z = −104 m in the HERA tunnel in the direction of the positron beam.

2.3 Triggering

Events were filtered online by a three level trigger system [21, 26]. At the first level, DIS events were selected by requiring a logical AND between two conditions based on energy deposits in the calorimeter. The first condition was the presence of an isolated electromagnetic energy deposit of greater than 2.5 GeV. The corresponding HAC energy was required to be either less than 0.95 GeV or no more than a third of the EMC energy. The threshold values have been chosen to give >99% efficiency for detecting positrons with energy greater than 5 GeV as determined by Monte Carlo studies. The second condition required that the EMC section have an energy deposit greater than 3.75 GeV. Background from protons interacting outside the detector was rejected using the time measurement of the energy deposits in the upstream veto counters and the SRTD.

At the second level trigger (SLT), background was further reduced using the measured times of energy deposits and the summed energies from the calorimeter. Events were accepted if

$$\delta_{SLT} \equiv \sum_i E_i(1 - \cos\theta_i) > 24 \text{ GeV} - 2E_\gamma \tag{3}$$

where E_i and θ_i are the energies and polar angles (with respect to the nominal vertex position) of calorimeter cells, and E_γ is the energy measured in the luminosity monitor photon calorimeter. For perfect detector resolution and acceptance, δ_{SLT} is twice the positron beam energy (55 GeV) for DIS events while for photoproduction events, where the scattered positron escapes down the beampipe, δ_{SLT} peaks at much lower values.

The full event information was available at the third level trigger (TLT). Tighter timing cuts as well as algorithms to remove beam-halo and cosmic muons were applied. The quantity δ_{TLT} was determined in the same manner as for δ_{SLT} and was required to be $\delta_{TLT} > 25 \text{ GeV} - 2E_\gamma$. Finally, DIS events were accepted if a scattered positron candidate of energy greater than 4 GeV was found.

3 Kinematics of exclusive ϕ production

Figure 1 shows a schematic diagram for exclusive ϕ production in the reaction

$$e^+p \to e^+\phi N, \tag{4}$$

where N represents either a proton or a diffractively dissociated nucleonic system of mass M_N. The kinematics are described by the following variables: the negative of the squared four-momentum transfer carried by the virtual photon[2] $Q^2 = -q^2 = -(k - k')^2$, where k (k') is the four-momentum of the incident (scattered) positron; the Bjorken variable $x = Q^2/2P \cdot q$, where P is the four-momentum of the incident proton; the variable which describes the energy transfer to the hadronic final state $y = q \cdot P/k \cdot P$; the c.m. energy, $\sqrt{s}$, of the ep system, where $s = (k + P)^2 \approx 4E_eE_p = (300\ \text{GeV})^2$; W, the c.m. energy of the γ^*p system: $W^2 = (q + P)^2 = Q^2(1 - x)/x + M_p^2 \approx ys$, where M_p is the proton mass; and $t' = |t - t_{min}|$, where t is the four-momentum transfer squared, $t = (P - P')^2$, from the photon to the ϕ, t_{min} is the maximum kinematically allowed value of t and P' is the four-momentum of the outgoing proton. The squared transverse momentum p_T^2 of the ϕ with respect to the photon direction is a good approximation to t' since t_{min} is small, $|t_{min}| \ll 10^{-2}$ GeV^2.

In this analysis, the ϕ was observed in the decay $\phi \to K^+K^-$. The three-momentum vector and energy (E_ϕ) of the ϕ was reconstructed from the kaon three-momenta as determined from the tracking detectors and assuming $K^\pm$ masses for the charged particles. The production angles (θ_ϕ and ϕ_ϕ) and momentum (p_ϕ) of the ϕ and the angles of the scattered positron ($\theta_e{}'$ and $\phi_e{}'$), as determined with the RCAL and SRTD, were used to reconstruct the kinematic variables x, Q^2, etc. Using energy and momentum conservation, the energy of the scattered positron was determined from the relation

$$E_e^c = [2E_e - (E_\phi - p_\phi cos\theta_\phi)]/(1 - cos\theta_e'). \tag{5}$$

This relation assumes that $M_N = M_p$ and that the transverse momentum of the proton is negligible compared to its longitudinal component. The resulting resolution of the energy of the positron at a typical energy of 26 GeV is less than 1% compared to the one of the direct measurement in the calorimeter of 5%. The variable y is calculated from the expression $y = (E_\phi - p_\phi cos\theta_\phi)/2E_e$. The calculation of p_T^2 also uses the momentum of the ϕ and the corrected positron momentum: $p_T^2 = (p_{ex} + p_{\phi x})^2 + (p_{ey} + p_{\phi y})^2$.

4 Event selection

The following off-line cuts were applied to select events from the reaction $\gamma^*p \to \phi(\to K^+K^-)N$:

- select a scattered positron with an energy, as measured in the calorimeter, greater than 5 GeV. The positron identification algorithm is based on a neural network using information from the CAL and is described elsewhere [27]. The efficiency of the identification algorithm is larger than 96% for the final data sample;

[2] In the Q^2 range covered by this data sample, effects due to Z^0 exchange can be neglected.

- select events with a scattered positron whose impact point in the SRTD was outside the square of 24×24 cm^2 centered on the beam axis or events with an RCAL impact point outside the square of 32×32 cm^2; this requirement controls the determination of the positron scattering angle;
- require $\delta = \sum_i E_i(1 - \cos\theta_i) > 35$ GeV, where the sum runs over all calorimeter cells; this cut reduces the radiative corrections;
- require exactly two oppositely charged tracks associated with a reconstructed vertex and not associated with the positron;
- require each track within the pseudorapidity[3] range $|\eta| < 1.75$ (corresponding to $20^o < \theta < 160^o$) and with a transverse momentum greater than 150 MeV. These cuts select the well understood and high efficiency region of the tracking detector;
- require that the Z coordinate of the vertex is in the range -50 to 40 cm;
- require $E_{CAL}/P_\phi < 1.5$, where E_{CAL} is the calorimeter energy excluding that due to the scattered positron and P_ϕ is the sum of the absolute values of the momenta of the two oppositely charged tracks. This cut suppresses backgrounds with additional calorimeter energy unmatched to the tracks;
- reject photon conversion candidates ($\gamma \to e^+e^-$). The cut rejected two events in the ϕ mass range;
- require $p_T^2 < 0.6\,\mathrm{GeV}^2$; this cut reduces the non-exclusive ϕ backgrounds. It also reduces background from proton dissociation which, from hadron-hadron diffractive scattering, is expected to have a flatter p_T^2 distribution;
- select $1.01 < M_{K^+K^-} < 1.03$ GeV. Figure 2a shows a plot of the invariant mass of the K^+K^- system and demonstrates ϕ production at the large values of Q^2 and W of this experiment.

Figure 2b shows a scatter plot of Q^2 versus x for the selected events. The acceptance at low Q^2 is limited by the requirement that the positron is well contained in the detector: the selected events are therefore restricted to $Q^2 > 4$ GeV^2. The analysis presented here is limited to the region $7 < Q^2 < 25$ GeV^2. The track cuts limit the y range to $0.02 < y < 0.20$ ($42 < W < 134$ GeV). A total of 43 events passed all of these selection requirements. These are shown as the shaded histogram in Fig. 2a.

5 Monte Carlo simulation and acceptance calculation

The reaction $e^+p \to e^+\phi p$ was modelled using the Monte Carlo generator, DIPSI [28], which describes elastic vector meson production in terms of pomeron exchange with the pomeron treated as a colourless two-gluon system [12]. The model assumes that the exchanged virtual photon fluctuates into a quark-antiquark pair which then interacts with the two-gluon system.

[3]The pseudorapidity η is defined as $\eta = -\ln[\tan(\frac{\theta}{2})]$.

The cross section is proportional to the square of the gluon momentum density in the proton. The generator DIPSI does not include radiative corrections.

The input vertex distribution was simulated in accordance with that measured for unbiased photoproduction events. The generated events were passed through the ZEUS detector and trigger simulation programs as well as through the analysis chain. The same offline cuts were used for the Monte Carlo events and for the data. Good agreement is found between the Monte Carlo and data for the distributions of the kinematic variables.

The simulated events were used to correct the data for acceptance. The acceptance includes the geometric acceptance, reconstruction efficiencies, detector efficiencies and resolution, corrections for the offline analysis cuts and a correction for the $M_{K^+K^-}$ cut. The acceptance is shown in Fig. 2c as a function of Q^2; in the region $7 < Q^2 < 25$ GeV^2, the acceptance varies between 44% and 70%. It drops sharply below $Q^2 = 4$ GeV^2 and it also drops at small and large y. The acceptance is fairly constant at about 60% as a function of y, p_T^2 or $M_{K^+K^-}$ in the selected kinematic region. The resolutions in the measured kinematic variables, as determined from the Monte Carlo events, are better than 4% for Q^2 and 2% for y, in the Q^2, y region of this analysis.

The radiative corrections affecting the measured cross sections were calculated analytically at various points in the $y - Q^2$ plane and were found to be (10-15)% for the selection cuts used in the analysis and for the Q^2 and W dependences found in the data. They are taken into account in the cross sections given below. The corrections were found to be the same for ϕ and ρ^0 production to within 1%.

6 Analysis, cross sections and results

6.1 Background estimates

Backgrounds to the exclusive reaction (2) are from ϕ events with additional undetected particles, from ρ^0 and ω production and from proton dissociation events where the system N in reaction (4) has a small mass M_N and does not deposit energy in the detector. Studies of the unpaired bunches determined the beam-gas background to be negligible. The photoproduction background is also found to be negligible because of the requirements on the y range of the measurement and the high energy for the scattered positron.

In order to estimate the non-resonant background, a non-relativistic Breit-Wigner (B-W), convoluted with a Gaussian, on a flat background is fit to the mass spectrum of Fig. 2a between 1.00 and 1.05 GeV. The B-W width was fixed at the Particle Data Group (PDG) value of 4.43 MeV [29]. The resulting ϕ mass is 1019.4 ± 0.4 MeV, to be compared with the PDG value of 1019.413 MeV. The r.m.s. of the Gaussian is found to be approximately 2 MeV, consistent with the resolution expected from tracking. The resulting background under the ϕ signal (1.01 to 1.03 GeV) is estimated to be $(14 \pm 7^{+4}_{-7})$%, where the first number is the statistical and the second the systematic uncertainty. The systematic error includes the uncertainties from varying the shape of the background and the mass region that is fitted.

Since the proton was not detected, the proton dissociation background contribution had to be subtracted. Due to the limited statistics, the percentage of proton dissociation background for

the ϕ events was assumed to be the same as that determined for the ρ^0 events, i.e. $(22 \pm 8 \pm 15)\%$ [9].

The overall factor to correct for background is then $\Delta = (0.86 \times 0.78 = 0.67 \pm 0.17)$. Unless explicitly stated otherwise, this background was subtracted as a constant fraction for the cross sections given below.

6.2 The ep cross section

The cross section, measured in the kinematic region defined above, is obtained from

$$\sigma(e^+p \to e^+\phi p) = \frac{\Delta}{C \cdot L_{int} \cdot B} \sum_{i=1}^{N} \frac{1}{A_i}, \tag{6}$$

where N (= 43) is the observed number of events after all cuts, Δ is the background correction factor, A_i is the bin-by-bin acceptance (which averages 58.7% as discussed above), L_{int} is the integrated luminosity of 2.62 pb^{-1}, $B = 0.491$ is the $\phi \to K^+K^-$ branching ratio [29] and C = 1.12 is the average correction for QED radiative effects. The corrected ep cross section for exclusive ϕ production at $\sqrt{s} = 300$ GeV is

$$\sigma(e^+p \to e^+\phi p) = 0.034 \pm 0.007\ (stat.) \pm 0.011\ (syst.)\ \text{nb},$$

integrated over the ranges $7 < Q^2 < 25$ GeV^2, $0.02 < y < 0.20$ and $p_T^2 < 0.6$ GeV^2.

The quoted systematic uncertainty is derived from the following (the corresponding value is given in parentheses):

- the E_{CAL}/P_ϕ cuts used to remove non-exclusive backgrounds were varied from 1.3 to 1.7. In an alternate background estimate, tracks were matched to the calorimeter energy deposits and events containing an unmatched cluster with energy in excess of 0.3 or 0.4 GeV were discarded (5%);
- the cut on the impact position of the positron was varied by 4 mm, the positron energy cut was varied and the δ cut was varied from 30 to 40 GeV (13%);
- the cuts on the tracks were varied. The lower cut on the transverse momentum was varied between 0.1 and 0.2 GeV and different polar angle selections were made (4%);
- the cuts on the $M_{K^+K^-}$ region were varied by $\pm$ 2 MeV (7%);
- cuts were applied to the opening angle between the two charged particles. Because of the low Q-value for the $\phi \to K^+K^-$ decay, the charged decay particles have a small opening angle. This study checks the simulation of the ability of the CTD to resolve two close tracks (5%);
- the cut on the vertex position was varied by 10 cm (5%);
- the Q^2, y, p_T^2 and helicity decay dependence in the DIPSI Monte Carlo model was varied (3%).

Adding these systematic uncertainties in quadrature (18%) to those from the background correction (25%), the luminosity determination and first level trigger efficiency (3.5%) and the radiative corrections (10%) yields 32% as the overall systematic uncertainty.

6.3 The $\gamma^* p$ cross sections

The ep cross section can be converted to a $\gamma^* p$ cross section as follows. The differential ep cross section for one photon exchange can be expressed in terms of the transverse and longitudinal virtual photoproduction cross sections as:

$$\frac{d^2\sigma(ep)}{dydQ^2} = \frac{\alpha}{2\pi y Q^2}\left[\left(1+(1-y)^2\right)\cdot\sigma_T^{\gamma^* p}(y,Q^2) + 2(1-y)\cdot\sigma_L^{\gamma^* p}(y,Q^2)\right].$$

The virtual photon-proton cross section can then be written in terms of the positron-proton differential cross section:

$$\sigma(\gamma^* p \to \phi p) = (\sigma_T^{\gamma^* p} + \epsilon\sigma_L^{\gamma^* p}) = \frac{1}{\Gamma_T}\frac{d^2\sigma(ep\to e\phi p)}{dydQ^2}, \tag{7}$$

where Γ_T, the flux of transverse virtual photons, and ϵ, the ratio of the longitudinal to transverse virtual photon flux, are given by

$$\Gamma_T = \frac{\alpha\,(1+(1-y)^2)}{2\pi y Q^2} \quad \text{and} \quad \epsilon = \frac{2(1-y)}{(1+(1-y)^2)}.$$

Throughout the kinematic range studied here, ϵ is in the range $0.97 < \epsilon < 1$.

Using Eq. (7), $\sigma(\gamma^* p \to \phi p)$ was determined with Γ_T calculated from the Q^2, x and y values on an event-by-event basis. The resulting cross sections in two ranges of Q^2 are

$$\sigma(\gamma^* p \to \phi p) = 10.3 \pm 2.2\ (stat.)\ \text{nb for } < Q^2 >= 8.2\ \text{GeV}^2 \text{ and } < W >= 94\ \text{GeV}$$

and

$$\sigma(\gamma^* p \to \phi p) = 3.1 \pm 0.7\ (stat.)\ \text{nb for } < Q^2 >= 14.7\ \text{GeV}^2 \text{ and } < W >= 99\ \text{GeV}.$$

The 32% overall systematic uncertainty on $\sigma(ep)$ applies to both values for $\sigma(\gamma^* p \to \phi p)$. After correcting for the different $< W >$ and assuming a Q^2 dependence of the form $Q^{-2\alpha}$ one finds $2\alpha = 4.1 \pm 1.2(\text{stat.})$. This value agrees, within errors, with the result found for the exclusive ρ^0 production $2\alpha = 4.2 \pm 0.8(\text{stat.})^{+1.4}_{-0.5}(\text{syst.})$ [9].

6.4 ϕ decay distribution

The ϕ s-channel helicity decay angular distribution, $H(\cos\theta_h, \phi_h, \Phi_h)$, can be used to determine the ϕ spin state [30], where θ_h and ϕ_h are the polar and azimuthal angles, respectively, of the K^+ in the ϕ c.m. system and Φ_h is the azimuthal angle of the ϕ production plane with respect to the positron scattering plane. The quantisation axis is defined as the ϕ direction in the $\gamma^* p$ c.m. system. After integrating over ϕ_h and Φ_h, the $\cos\theta_h$ decay angular distribution, shown in Fig. 2d, can be written as:

$$\frac{1}{N}\frac{dN}{d\cos\theta_h} = \frac{3}{4}[1 - r_{00}^{04} + (3r_{00}^{04} - 1)\cos^2\theta_h], \tag{8}$$

where r_{00}^{04} is a particular linear combination of density matrix elements and represents the probability that the ϕ is produced in the helicity zero state.

A maximum likelihood fit of the helicity $\cos\theta_h$ distribution in the range[4] $|\cos\theta_h| < 0.8$ to the form of Eq. (8) yields $r_{00}^{04} = 0.76^{+0.11}_{-0.16} \pm 0.12$ at $< Q^2 > = 12.3$ GeV^2 and $< W > = 98$ GeV. This was not corrected for background, since the dominant contribution is from ϕ production with proton dissociation, which is expected to have a similar helicity. The first uncertainty is statistical, and the second is derived from the variations of the result when different ranges in $\cos\theta_h$ were used in the fit, when the systematic studies of section 6.2 were used or when a flat background of 15% was included. This result is in sharp contrast to the measurement at $Q^2 = 0$ [4], where r_{00}^{04} is compatible with zero, and indicates that the cross section for $\gamma^* p \to \phi p$ is dominated by ϕ's in the helicity zero state. If s-channel helicity conservation (SCHC) is assumed, then $R = \sigma_L/\sigma_T = r_{00}^{04}/\epsilon(1 - r_{00}^{04})$. For DIS ρ^0 production, $r_{00}^{04} = 0.6 \pm 0.1^{+0.2}_{-0.1}$ [9]. For the NMC ϕ data $r_{00}^{04} = 0.84 \pm 0.18$ and $\epsilon = 0.75$ [19].

6.5 The W dependence of the $\gamma^* p \to \phi p$ cross section

Figure 3 shows a compilation [2, 19, 31, 32, 33] of photoproduction and selected leptoproduction exclusive ϕ cross sections. In this figure the cross section

$$\sigma_T(\gamma^* p \to \phi p) + \sigma_L(\gamma^* p \to \phi p) = \frac{(1+R)}{(1+\epsilon R)} \cdot \sigma(\gamma^* p \to \phi p) = (1 - r_{00}^{04} + \frac{r_{00}^{04}}{\epsilon}) \cdot \sigma(\gamma^* p \to \phi p) \qquad (9)$$

is plotted as a function of W. To obtain R, SCHC has been assumed, as discussed above. In Fig. 3, the cross sections at $Q^2 = 0$ are shown assuming $R = 0$. The results obtained in this analysis are shown at a mean flux-weighted Q^2 of 8.2 and 14.7 GeV^2, respectively. To compare with the NMC cross sections[5] the NMC values were scaled to $Q^2 = 8.2$ (14.7) GeV^2 from $Q^2 = 7.23$ (11.35) GeV^2 using their measured $Q^{-4.54\pm0.78}$ dependence and $\epsilon = 0.75$ was used. In addition, the NMC deuterium data have been corrected to obtain ϕ production off a nucleon using a factor[6] of 0.94±0.02 [18]. To compare with results from the NMC experiment, which has determined exclusive ϕ cross sections integrated over all p_T^2, a 4.5% correction is applied to the ZEUS data to account for the cross section in the p_T^2 range between 0.6 and 1.0 GeV^2 based on the slope of the distribution measured in the ρ^0 analysis [9].

The $\gamma p \to \phi p$ cross section for real ($Q^2 = 0$) photons [4] shows only a slow rise, consistent with soft pomeron exchange (as shown by the dashed line which represents a $W^{0.22}$ dependence). At medium Q^2 (< 8 GeV^2), no high energy data are yet available. At higher Q^2, the ZEUS values of the cross sections are significantly larger than those of the NMC experiment.

Figure 3 shows that the cross sections rise strongly with increasing W. At $Q^2 = 8.2$ and 14.7 GeV^2, the strong increase in the $\gamma^* p \to \phi p$ cross sections between 12 (NMC data) and 100 GeV (ZEUS data) is in contrast to that expected from the Donnachie and Landshoff model [35] based on the energy dependence given by the soft pomeron. However, it is similar to that observed previously for the DIS ρ^0 production [9] and for J/ψ photoproduction [8]. It is also in qualitative agreement with pQCD calculations in which vector meson production is related to

[4]Backgrounds due to photon conversions and $\rho^0 \to \pi^+\pi^-$ tend to populate the regions $|\cos\theta_h| > 0.8$.

[5]Since the EMC [20] and NMC data cover approximately the same kinematic region, the more recent NMC data [19] have been chosen to make comparisons.

[6]If instead, one corrects [33] for the incoherent contribution (0.77±0.10) as well as a d/p (normalised per nucleon) ratio of 0.77± 0.21, as measured by E665 [34], one obtains a factor of 1.0±0.3. These measurements are for ρ^0 production and the ϕ data are assumed to behave in a similar manner.

the square of the gluon momentum density [13, 18]. As displayed in Eq. (1), these calculations are for only the longitudinal part of the forward differential cross section.

A functional dependence $\sigma \sim W^k$ with $k = 0.92 \pm 0.08 \pm 0.16$ has recently been obtained for the inclusive $\gamma^* p \rightarrow X + N$ diffractive scattering cross sections for excitation masses M_X up to 15 GeV [11]. The exclusive DIS ϕ vector meson data show a similar behaviour (see the solid line in Fig. 3 which is a $\sim W^{0.9}$ dependence).

6.6 The ratio of ϕ to ρ^0 production

The ratio of the production cross sections for ϕ and ρ^0 may be determined using the previously published ρ^0 measurement [9]. Scaling the ρ^0 data to the same $< Q^2 >$ and $< W >$ with a $Q^{-4.2}$ and $W^{0.8}$ dependence, and with the assumption that the proton dissociation background and the radiative corrections are identical, a value of $\sigma(\phi)/\sigma(\rho^0) = 0.18 \pm 0.05$ (stat.) $\pm$ 0.03 (syst.) is obtained at $< Q^2 > = 12.3$ GeV^2 and $< W > = 98$ GeV. The statistical error comes from adding in quadrature the statistical errors for the ϕ and the ρ^0 [9] cross sections. The systematic error comes from combining in quadrature the systematic errors for the ϕ and the ρ^0 [9]. The correlated uncertainties which include contributions from the proton dissociation background and radiative corrections are excluded. This result is shown in Fig. 4 as a function of Q^2 along with similar data from the NMC experiment [19, 33]. Also shown is a recent determination at $W \approx 70$ GeV and $Q^2 \approx 0$ [4] giving $\sigma(\phi)/\sigma(\rho^0) = 0.065 \pm 0.013$ (stat.). As previously noted by the EMC experiment [20], the ratio for Q^2 values between 2 and 10 GeV^2 is larger than that at $Q^2 \approx 0$. The measurement from ZEUS is consistent with the value of 2/9 expected from the quark charges and a flavour independent production mechanism.

7 Summary

Exclusive ϕ production has been studied in deep inelastic $e^+ p$ scattering at Q^2 values between 7 and 25 GeV^2 and in the $\gamma^* p$ centre of mass energy (W) range from 42 to 134 GeV. The $\gamma^* p \rightarrow \phi p$ cross sections at these large Q^2 values are significantly larger than the NMC results, indicating a strong dependence on W between the lower NMC energy and HERA, in contrast to the behaviour of the elastic ϕ photoproduction cross section.

The dependence is similar to that observed for the reaction $\gamma^* p \rightarrow \rho^0 p$ and for the elastic photoproduction of the J/ψ and is in qualitative agreement with the strong energy dependence expected from pQCD calculations [12, 13, 17] which relate these cross sections to the rise in the gluon momentum density in the proton at small x. A steep W dependence is also observed in inclusive DIS diffractive scattering [11] and in the $\gamma^* p$ total cross section[15].

The data suggest that the cross section for exclusive vector meson production by real or virtual photons has a strong energy dependence at large W-values whenever a hard scale (Q^2 or $M^2_{J/\psi}$) is present. The ratio of $\sigma(\phi)/\sigma(\rho^0)$ of $0.18 \pm 0.05 \pm 0.03$ at $< Q^2 >$ of 12.3 GeV^2 is significantly larger than the value observed in photoproduction at the same W and is approaching the expected value of 2/9.

8 Acknowledgements

We thank the DESY Directorate for their strong support and encouragement. The remarkable achievements of the HERA machine group were essential for the successful completion of this work and are gratefully appreciated. We also acknowledge the many informative discussions we have had with L. Frankfurt, P. Landshoff, A. Sandacz and M. Strikman.

References

[1] T.H. Bauer et al., Rev. Mod. Phys. 50 (1978) 261.

[2] J. Busenitz et al., Phys. Rev. D40 (1989) 1.

[3] R.M. Egloff et al., Phys. Rev. Lett. 43 (1979) 657.

[4] ZEUS Collab., M. Derrick et al., DESY 96-002, to be published in Phys. Lett. B (1996).

[5] A. Donnachie and P.V. Landshoff, Nucl. Phys. B244 (1984) 322;
Phys. Lett. B296 (1992) 227.

[6] ZEUS Collab., M. Derrick et al., Z. Phys. C63 (1994) 391;
H1 Collab., S. Aid et al., Z. Phys. C69 (1995) 27.

[7] ZEUS Collab., M. Derrick et al., Z. Phys. C69 (1995) 39;
H1 Collab., S. Aid et al., DESY 95-251.

[8] H1 Collab., T. Ahmed et al., Phys. Lett. B338 (1994) 507;
ZEUS Collab., M. Derrick et al., Phys. Lett. B350 (1995) 120.

[9] ZEUS Collab., M. Derrick et al., Phys. Lett. B356 (1995) 601.

[10] H1 Collab., S. Aid, DESY 96-023 (1996).

[11] ZEUS Collab., M. Derrick et al., DESY 96-018, to be published in Z. Phys. C (1996).

[12] M. G. Ryskin, Z. Phys. C57 (1993) 89.

[13] S. J. Brodsky et al., Phys. Rev. D50 (1994) 3134.

[14] J. R. Forshaw and M. G. Ryskin, Z. Phys. C68 (1995) 137;
J. Bartels et al, DESY 95-253 (1995).

[15] ZEUS Collab., M. Derrick et al., Z. Phys. C65 (1995) 379;
H1 Collab., T. Ahmed et al., Nucl. Phys. B439 (1995) 471.

[16] H. Joos, Acta Physica Austriaca, Suppl. IV (1967) 320.

[17] H. Abramowicz et al., DESY 95-047 (1995); M. Strikman, private communication.

[18] L. Frankfurt, W. Koepf and M. Strikman, TAUP-2290-95, hep-ph/9509311 (1995).

[19] NMC Collab., M. Arneodo et al., Nucl. Phys. B429 (1994) 503.

[20] EMC Collab., J. Ashman et al., Z. Phys. C39 (1988) 169.

[21] ZEUS Collab., The ZEUS Detector Status Report 1993;
ZEUS Collab., M. Derrick et al., DESY 95-193 (1995).

[22] C. Alvisi et al., Nucl. Instr. Meth. A305 (1991) 30.

[23] C. B. Brooks et al., Nucl. Instr. Meth. A283 (1989) 477;
B. Foster et al., Nucl. Instr. Meth. A338 (1994) 254.

[24] M. Derrick et al., Nucl. Instr. Meth. A309 (1991) 77;
A. Andresen et. al., Nucl. Instr. Meth. A309 (1991) 101;
A. Bernstein et. al., Nucl. Instr. Meth. A336 (1993) 23.

[25] D. Kisielewska et al., DESY-HERA 85-25 (1985);
J.Andruszków et al., DESY 92-066 (1992).

[26] W. H. Smith et al., Nucl. Instr. Meth. A355 (1995) 278.

[27] H. Abramowicz, A. Caldwell and R. Sinkus, Nucl. Instr. Meth. A365 (1995) 508;
R. Sinkus, Ph. D. Thesis, University of Hamburg, 1996.

[28] M. Arneodo, L. Lamberti and M. G. Ryskin, submitted to Comp. Phys. Comm. (1995).

[29] Review of Particle Properties, Particle Data Group, L. Montanet et al., Phys. Rev. D50 (1994) 1173.

[30] K. Schilling, P. Seyboth and G. Wolf, Nucl. Phys. B15 (1970) 397;
K. Schilling and G. Wolf, Nucl. Phys. B61 (1973) 381.

[31] S.I. Alekhin et al., CERN-HERA 87-01 (1987);
"Total Cross-Sections for Reactions of High Energy Particles", Landolt-Börnstein, New Series, Vol. 12b, editor H. Schopper (1987).

[32] D. G. Cassel et al., Phys. Rev. D24 (1981) 2787.

[33] A. Sandacz, private communication.

[34] Fermilab E665 Collab., M. R. Adams et al., Phys. Rev. Lett. 74 (1995) 1525.

[35] A. Donnachie and P. V. Landshoff, Nucl. Phys. B311 (1989) 509;
Phys. Lett. B185 (1987) 403;
Phys. Lett. B348 (1995) 213.

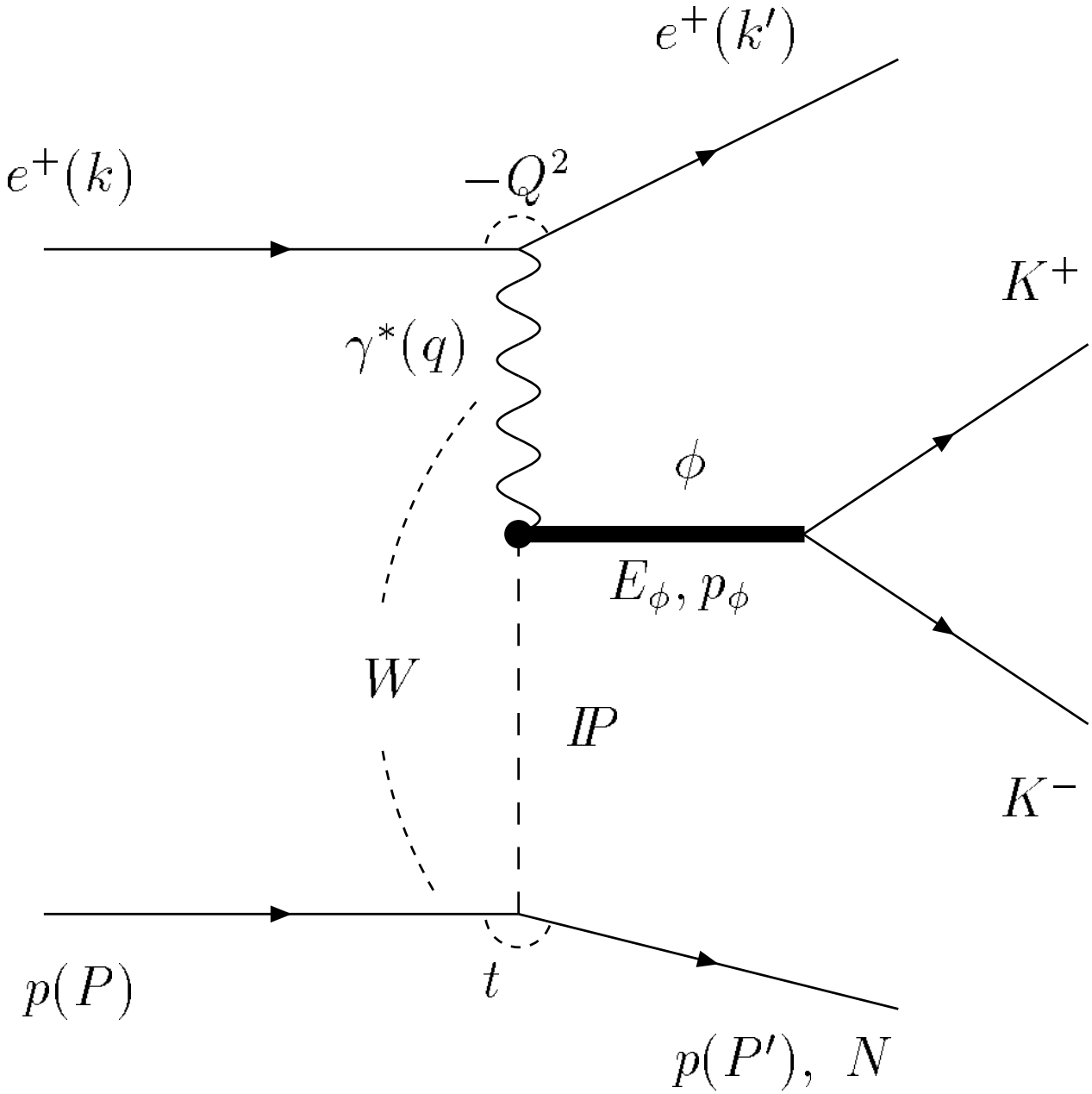

Figure 1: Schematic diagram of exclusive ϕ production in deep inelastic e^+p interactions.

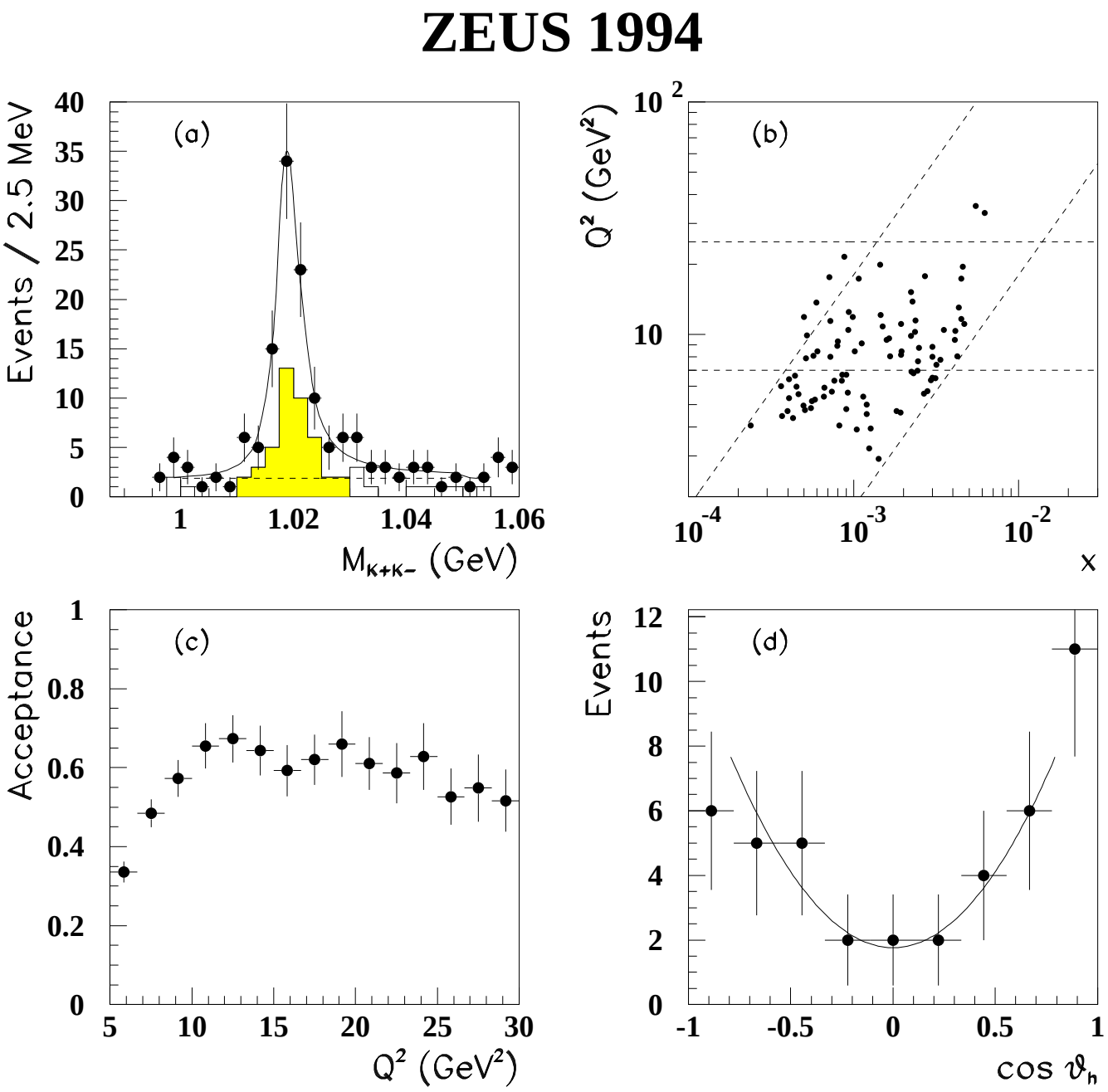

Figure 2: (a) The invariant mass distribution for the K^+K^- pairs; the curves are the best fit to a Breit-Wigner convoluted with a Gaussian (solid line) over a flat background (dashed line). The events in the $y - Q^2$ region of this analysis are shown as the hatched histogram; (b) a scatter plot of Q^2 versus x for the ϕ events. The lines correspond to the region in Q^2 and y selected for this analysis; (c) the acceptance for DIS ϕ production as a function of Q^2 for events in the y range of the cross section measurements; (d) the cosθ_h helicity angular distribution for candidate events. The acceptance in cosθ_h is flat over the region $|\cos\theta_h| < 0.8$. The curve shows the result of the maximum likelihood fit for events in this range as described in the text.

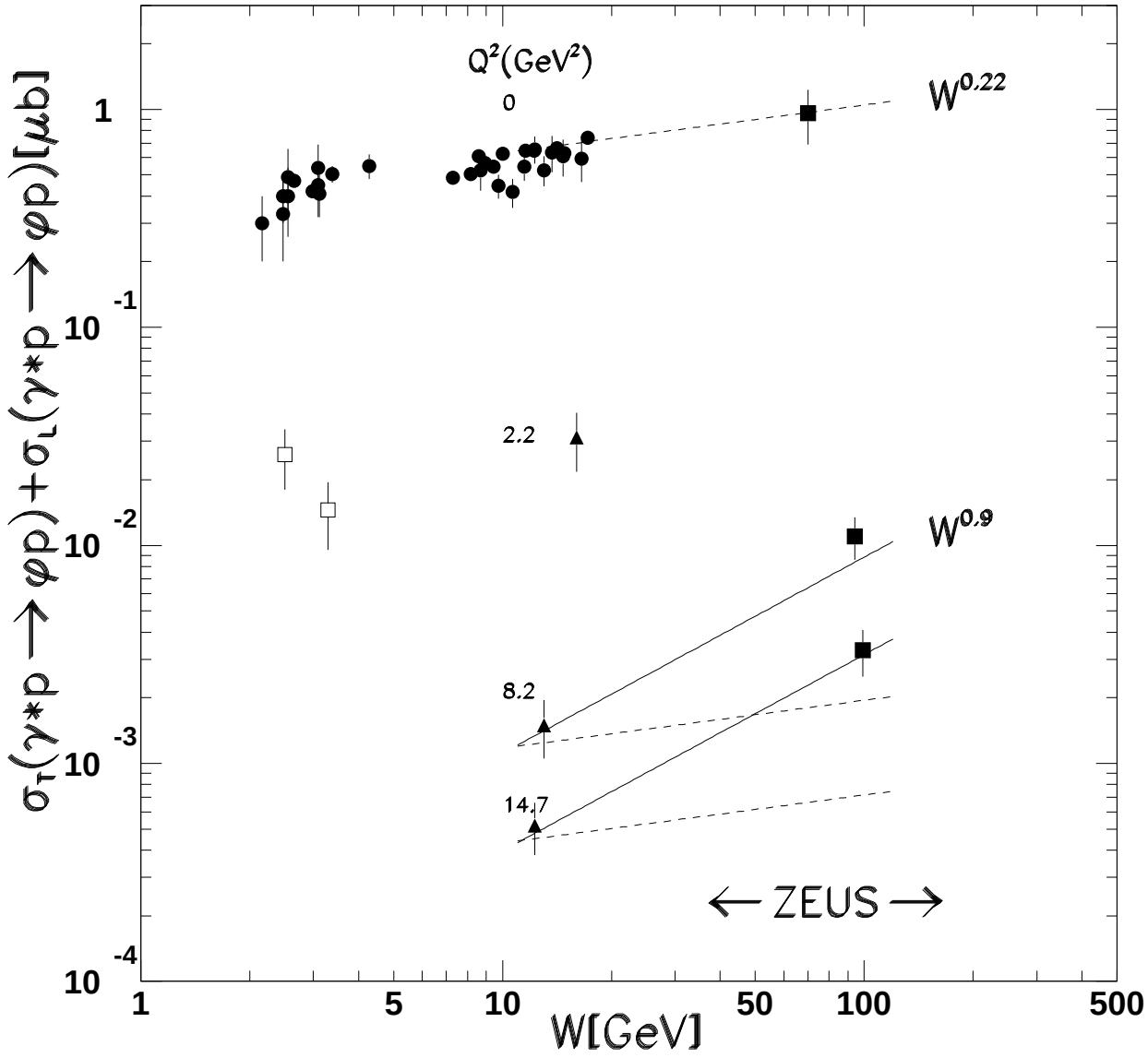

Figure 3: The $\gamma^* p \to \phi p$ cross section $(\sigma_T + \sigma_L)$ as a function of W, the $\gamma^* p$ centre of mass energy, for several values of Q^2. The low energy data ($W < 20$ GeV, solid dots, open squares and solid triangles) come from fixed target experiments [2,19,31-33]. The high energy data ($W > 50$ GeV, solid squares) come from the ZEUS experiment [4] and the present analysis . The ZEUS data at $Q^2 = 8.2$ and 14.7 GeV^2 have an additional correlated systematic uncertainty of 32% (not shown); the data from Refs. [19](solid triangles) and [32](open squares) have additional 20% and 25% normalisation uncertainties, respectively. The photoproduction data are shown assuming $R = 0$. The NMC data [19] are scaled to the ZEUS Q^2 values as described in the text. The dashed and solid lines are drawn to guide the eye.

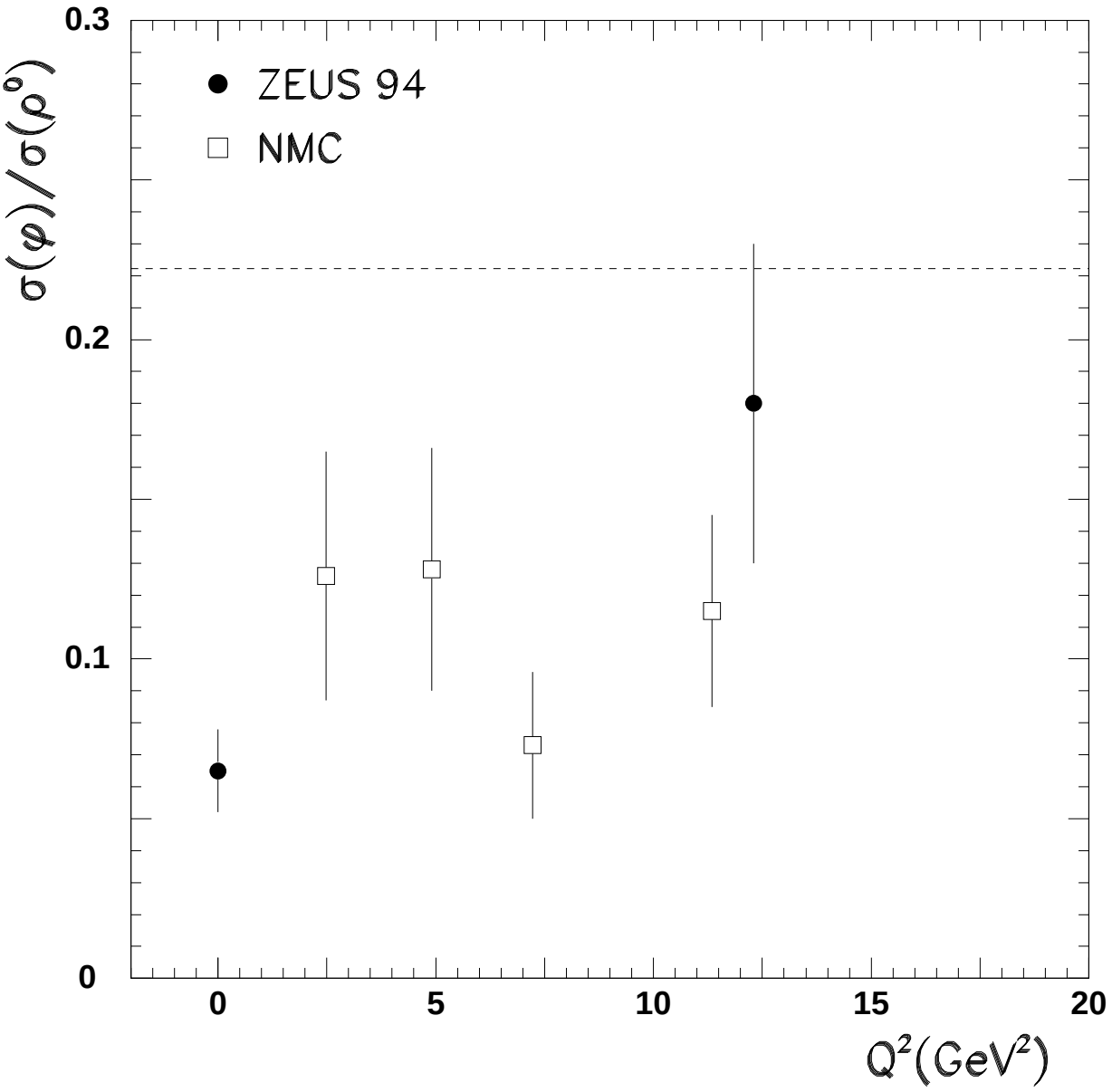

Figure 4: The ratio of the cross section for exclusive ϕ to ρ^0 production is shown as a function of Q^2. The point at $Q^2 = 12.3$ GeV^2 is from the present analysis. Only the statistical error is shown. There is an additional systematic error of 15% arising from the different systematic errors for the ϕ and ρ^0 analyses. The point at $Q^2 \approx 0$ is also from this experiment [4]. Also shown in the figure are data from the NMC collaboration [19]. Note that the ZEUS and NMC data points are at different $\gamma^* p$ c.m. energies (W), with the ZEUS data having $< W > \approx 100$ GeV while the NMC data points are at $< W > \approx 15$ GeV. The horizontal dashed line shows the value of 2/9 expected at high Q^2 (see text).